

Carbon Nanotube Fiber Microelectrodes Show a Higher Resistance to Dopamine Fouling

Wolfgang Harreither,^{†,§} Raphaël Trouillon,[†] Philippe Poulin,[‡] Wilfrid Neri,[‡] Andrew G. Ewing,^{†,#} and Gulnara Safina^{*,†}

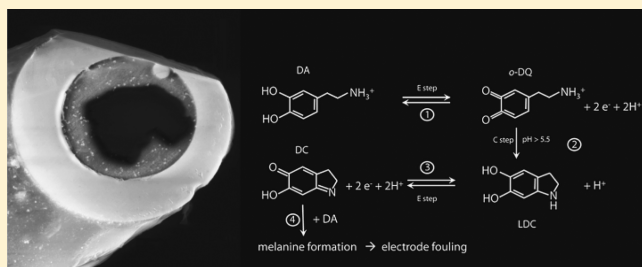
[†]Department of Chemistry and Molecular Biology, University of Gothenburg, Gothenburg 41296, Sweden

[‡]Centre de Recherche Paul Pascal, CNRS, Université de Bordeaux, Pessac 33600, France

[#]Department of Chemical and Biological Engineering, Chalmers University of Technology, Gothenburg 41296, Sweden

Supporting Information

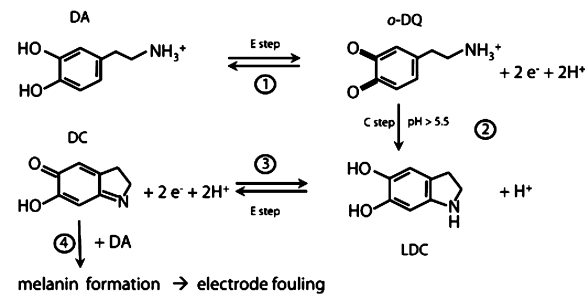
ABSTRACT: We have compared the properties and resistance to DA fouling of a carbon nanotube fiber (CNTF) microelectrode to a traditional carbon fiber (CF) microelectrode. These two materials show comparable electrochemical activities for outer-sphere and inner-sphere redox reactions. Although the CNTF might have a higher intrinsic RC constant, thus limiting its high-frequency behavior, the CNTF shows a significantly higher durability than the CF in terms of electrode stability. During constant oxidation of 100 μM DA, the signal measured by the CNTF microelectrode shows a 2-h window over which no decrease in current is observed. Under the same conditions, the current obtained at the CF microelectrode decreases by almost 50%. A model of the fouling process, assuming the formation of growing patches of insulator on the surface, has been compared to the data. This model is found to be in good agreement with our results and indicates a growth rate of the patches in the 0.1–2 nm s⁻¹ range.



Dopamine (DA) is an important neurotransmitter involved in reward and addiction mechanisms.^{1,2} The detection and quantification of this substance is needed to elucidate the pathways responsible for these functions. Since DA is electroactive, electrochemical detection is an attractive method for its monitoring *in vitro* and *in vivo* and has been routinely performed since the seminal work of Ralph Adams published in the 1970s.³ Exogenous and endogenous levels of neurotransmitters have been measured both with continuous amperometry and fast scan cyclic voltammetry (FSCV).^{4–8} FSCV offers the possibility of carrying out precise chemical identification and is therefore extensively used as an analytical technique for neurochemical research. Interestingly, despite its decreased chemical resolution, steady state amperometry is still a popular electrochemical technique for biological assays because of its capability to perform quantitative *in situ* measurements with excellent, submillisecond, time resolution.

The products of DA oxidation are very reactive and may form an insulating film on the electrode surface, thus jeopardizing the long-term stability of the electrode.^{9–12} The reaction pathway of DA fouling is shown in Scheme 1.^{9,10} The electrochemical oxidation of DA proceeds via a two-electron transfer forming the o-dopaminoquinone (o-DQ) (1). Subsequently, this intermediate undergoes an intramolecular addition when the amine is protonated, resulting in a cyclization leading leucodopaminochrome (LDC) (2). LDC undergoes a two-electron oxidation to form dopaminochrome (DC). DC may polymerize to melanin on the electrode by a

Scheme 1. Fouling Mechanism during Electrochemical Oxidation of DA in Aqueous Solutions



free radical polymerization, significantly inhibiting the surface dependent redox chemistry of DA.

The low cost, wide potential window and electroactivity for a variety of redox reactions of carbon materials makes them highly attractive for electroanalytical chemistry. Carbon shows a great diversity as an electrode material, stemming largely from its structural polymorphism, chemical stability, rich surface chemistry, and strong carbon–carbon bonds.¹³

Carbon fibers (CF) have been used for *in vivo* electrochemistry due to their small size and their good electroactivity

Received: May 8, 2013

Accepted: June 22, 2013

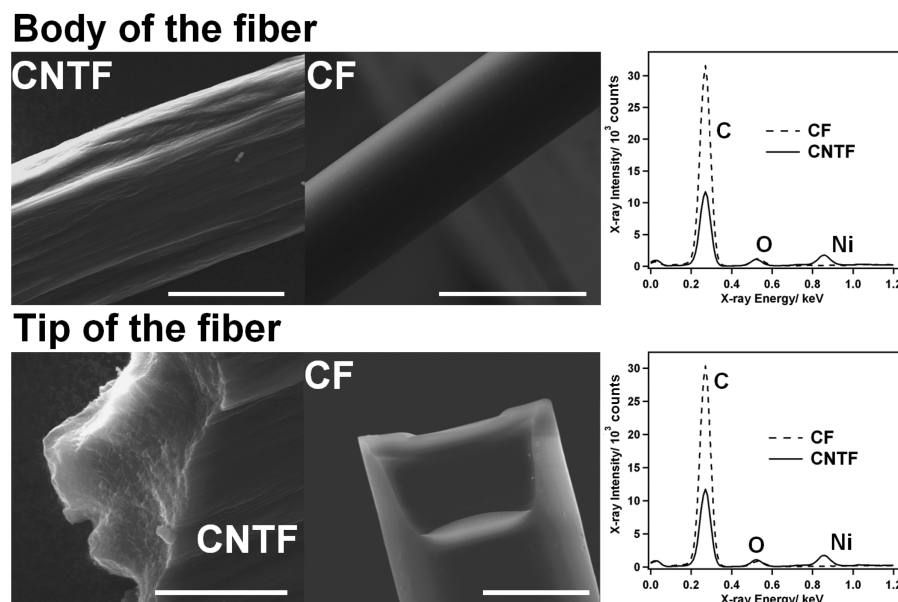


Figure 1. Characterization of the CNTF and CF: the top row shows SEM images of the body of the CNTF and CF (the bar indicates $50\text{ }\mu\text{m}$). These images clearly show the irregular surface of the CNTF, composed of several bundles of CNT, in contrast with the smooth surface of the CF. The right panel shows the EDX spectra obtained from the body of the CNTF (solid line) and CF (dotted line). The bottom row shows SEM images of the tip of the CNTF and CF (the bar indicates $20\text{ }\mu\text{m}$). The native CNTF shows individual CNT protruding at the fracture site. On the opposite, the CF shows a very homogeneous structure. The right panel shows the EDX spectra obtained from the tip of the CNTF (solid line) and CF (dotted line).

for a variety of biochemicals, such as neurotransmitters.^{14,15} However, CF, like glassy carbon, is affected by the fouling caused by the oxidation products of neurotransmitters. This issue strongly jeopardizes the quality of the measurements, as the electrochemical oxidation of neurotransmitters is typically an inner sphere reaction involving surface adsorption.¹⁶ Modified waveforms^{7,17} or membrane coatings^{18,19} have been proposed to improve the stability of carbon fiber electrode surfaces during FSCV measurements. However, maintaining a stable surface for amperometric detection, with fast reaction kinetics, is still a challenging issue. An another carbon material, boron-doped diamond (BDD) is known to exhibit a high chemical stability, at the expense of decreased reaction kinetics in comparison to other carbon materials.^{20,21} Carbon nanotubes (CNTs) have distinct structural and electronic properties compared with conventional carbon materials used in electrochemistry such as glassy carbon, graphite, and CF. CNTs exhibit a high aspect ratio, nanometer sized dimensions, good electrical conductivity, resistance against surface fouling, and a good biocompatibility.^{13,22–28} The outstanding mechanical and unique physical properties of individual CNTs have motivated the development of macrostructures based on CNTs, such as CNT arrays, films, and fibers.^{29–31} Such composite materials can be handled more conveniently than individual CNT and are therefore the attractive candidates for microelectrode materials.^{32,33}

In this report, we evaluate the electrochemical properties and resistance to fouling of carbon nanotube fiber (CNTF) and CF microelectrodes. Unlike BDD substrates, the CNTF were found to combine a high electroactivity and fast response, comparable to the ones observed with CF, together with a high chemical stability. The fiber format of this material also makes it easy to use and apply to electrode fabrication. The fouling resistance, evaluated from the time required to decrease by 50% the current measured under fouling conditions, has been found

to be up to three times higher than for the traditional CF electrode. The CNTF microelectrodes presented in this work exhibit an efficient electrochemical response with high resistance against chemical fouling. Unlike most of the alternatives to CF, these CNTF electrodes are easy to handle, as their dimensions are comparable to the traditionally used CF. Furthermore, the fiber format allows them to be cut, glued, and beveled, just like the traditional CF. These results suggest that this material is a potential and user-friendly candidate for the reliable *in situ* analysis of neurotransmitters. Additionally, we suggest in this report a model for the fouling phenomenon, where the electrode is blocked by growing patches of insulating material. This model was found to be in good agreement with the observed current decrease and suggests a growth rate of the insulating patches of $0.1\text{--}2\text{ nm s}^{-1}$.

EXPERIMENTAL SECTION

Reagents. The chemicals, of analytical grade, were obtained from Sigma-Aldrich (unless stated otherwise) and used as received. All solutions were made using $18\text{ M}\Omega\text{cm}$ water from a Millipore purification system, and the solutions pH was adjusted to 7.4 with concentrated NaOH.

CNTF Synthesis. The CNTF were prepared following previously published methods.^{32–34}

Briefly, 0.3 wt % of HipCO single wall CNTs (CNI, Houston, TX, USA) are dispersed in water using 1 wt % sodium dodecyl sulfate as the dispersant. (*Safety precautions!* Nanotubes were weighed and dispersed in a liquid under a Flowsciences Inc. vented hood that has HEPA filters. Gloves, glasses, and filtering facepiece (FFP3) masks are recommended while handling the raw powders of nanotubes.) The CNT dispersions were homogenized by tip-sonication. The fibers were spun continuously by injection of the homogeneous CNT dispersion in the coflowing stream of an aqueous solution of poly(vinyl alcohol) (PVA; 5 wt %, MW 195,000, hydrolysis

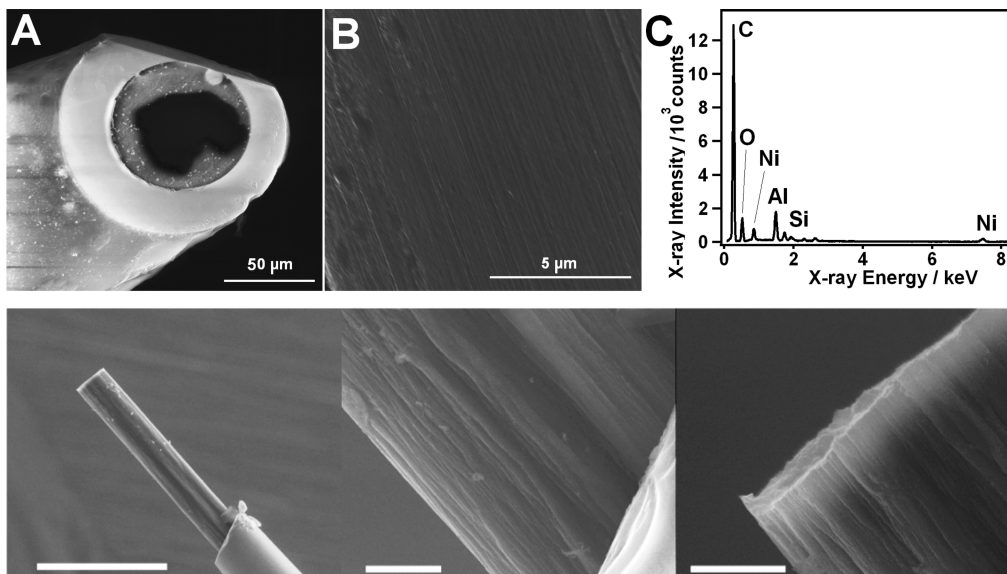


Figure 2. Surface characterization of the CNTF microelectrodes. The top row shows A: SEM images of a disk CNTF microelectrode; B: magnification of the smooth polished CNTF surface obtained at the center of the electrode presented on A; C: typical EDX spectra of a CNTF surface, taken at the center of the CNTF electrode surface. For comparison, the bottom row shows SEM images of a CNTF cylindrical electrode. The left picture shows a wide view of the device (the bar indicates 200 μm). The middle and right images show close ups of the device, respectively at the CNTF/glass interface and at the tip of the fiber (the bar indicates 10 μm).

99%). Subsequently the fibers were washed in pure water, dried, and then heat-treated at 600 °C for 6 h under argon atmosphere to fully eliminate the PVA.

Electrode Fabrication. The CNTF was cut to a length of approximately 5 mm, then inserted in a pulled glass capillary, and dipped into an epoxy resin bath to seal it. The electrode was cured at 100 °C overnight in the oven. Finally, the electrode tip was polished to an angle of 45° using a microelectrode beveler (Sutter Instrument Co., Novato, CA, USA), rinsed carefully, and sonicated in deionized water for 10 s. (Safety precautions! Gloves, glasses, and FFP3 masks are recommended as protection from inhaling the micro- and nanoparticles, which may form during electrode fabrication and polishing processes.) Electrical contact between the carbon fiber and a silver wire was established by inserting pieces of Wood's metal into the capillary and melting them. Disk carbon fiber (diameter: 33 μm) electrodes used for comparison were prepared as described in the literature.^{35,36}

Scanning Electron Microscopy and Energy Dispersive X-ray Spectroscopy. The dimensions and morphology of CNTF were characterized using a scanning electron microscope (SEM) FEI Quanta 200 equipped with a field emission gun (Tokyo, Japan). The instrument was operated at 20 kV accelerating voltage. The secondary electron images were obtained using the large field detector and the Everhart-Thornley detector. The elemental composition of a material at various measurement points was analyzed using an energy dispersive X-ray (EDX) system operated by Inca and AZtec softwares (Oxford Instruments). The contrast of the images was enhanced using an image processing software.

Electrochemical Characterization. All measurements were performed at room temperature. Cyclic voltammetry and amperometry were performed using a CHI 1030B potentiostat (CH Instruments, Austin, TX, USA). A standard three electrode configuration was used with a Ag|AgCl (3 M KCl) reference electrode (BASi, West Lafayette, IN, USA) and platinum wire as counter electrode. The buffer, used as the

supporting electrolyte, was carefully purged with nitrogen prior to experiments.

Simulations. The finite element modeling simulations were performed using Comsol Multiphysics 4.0 a. The system was simplified to facilitate the computation by drawing a square (edge length: 16 μm) partially blocked by insulating squares of edge d, as shown in the Supporting Information (Figure S1A), at the bottom of a cylinder (radius: 500 μm , height: 500 μm) of liquid, containing 1 mM of analyte, representing the electrochemical cell. The system was solved, assuming steady state, and the normal flux of analyte at the surface of the electrode was obtained. The calculations and fitting routines were performed with Igor Pro (Wavemetrics, US).

RESULTS AND DISCUSSION

Characterization of the Native Fibers. The morphologies of the native (before the electrode preparation) CNTF and CF were investigated with SEM. As shown in Figure 1, the CNTF shows an obvious composite structure. The surface of the cylindrical fiber is very irregular, and individual CNT can be observed at the tip of the fiber. That is in good agreement with previous microscopic observations of this type of fiber.³⁴ On the opposite, the structure of the CF was found to be highly homogeneous, and no specific organization could be observed in our SEM images.

Additionally, EDX analysis was performed at the body and tip of the CNTF and CF. The spectra were comparable for the body and the tip of the fibers, indicating the uniform chemical composition of these materials. The nickel peak could be observed at 0.85 keV in the case of CNTF, indicating the presence of the catalyst in the bulk of the material. The oxygen peak obtained at 0.52 keV indicates a high content in oxygen functionalities in the CNTF material as well as in the CF. This observation would be in good agreement with a high density of edge plane sites or defects, likely to host oxygen functionalities, in the CNTF.³⁷

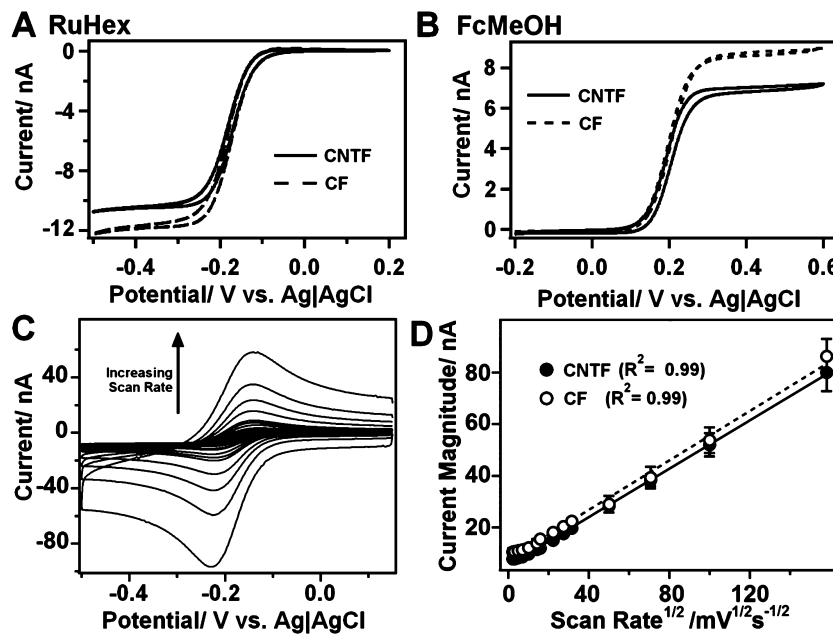


Figure 3. Typical CVs obtained for different outer-sphere redox probes with a CNTF microelectrode (solid line) and a CF microelectrode (broken line). A: 1 mM ruthenium hexaammine(II) chloride (RuHex) in PBS buffer pH 7.4; B: 1 mM ferrocenemethanol (FcMeOH) in PBS buffer pH 7.4; C: typical CVs of 1 mM RuHex in PBS buffer obtained with a CNTF for different scan rates (5, 10, 25, 50, 100, 200, 250, 500, 750, 1000, 2500, 5000, 10000, and 25000 mV s⁻¹); D: linear fits of the peak currents obtained for CNTF (black dots) and CF (white dots) microelectrodes in 1 mM RuHex in PBS buffer pH 7.4 versus the square root of the scan rate.

Characterization of the CF and CNTF Electrodes. The CNTF disk microelectrodes were prepared in a similar way to CF microelectrodes, with the exception that the CNTF was inserted in a prepulled glass capillary.

The resulting CNTF microelectrodes were first investigated using SEM as shown in Figure 2A and B. The morphology of the CNTF is quite different from a conventional CF showing highly fractured fiber-flanks. As a result the active surface of the electrode does not have a well-defined radius. From the micrographs, obtained for 3 electrodes, and taking into account the 45° beveling, an approximate diameter of $35 \pm 6 \mu\text{m}$ was measured. This result is very close to the diameter of the CF, hence ensuring the results obtained from the electrochemical characterization are comparable. Additionally, the edge of the CNTF usually shows a rough surface due to its composite nature (Figure 1). Because of the fine polishing induced by the beveling, this structure disappears after the electrode preparation (Figure 2B) as the electrode surface appears to be flat and smooth. CNTF was also used to make cylindrical electrodes. Figure 2 shows electron micrographs obtained at a smooth polished tip of the disk electrode (top row) and at a rough surface of the body and the tip of the intact (unpolished) cylindrical electrode (bottom row).

In Figure 2C, the elemental composition of the CNTF, obtained from EDX analysis, is shown. The EDX spectra were not significantly different from the ones obtained at the native fibers, thus indicating that the electrode fabrication process does not alter the material. The major EDX signal at 0.28 keV is attributed to carbon, and an oxygen peak is still observed at 0.52 keV. The peak observed at 1.74 keV indicates the presence of silicon and corresponds to the residuals of glass initially insulated the CNTF and remained on the carbon surface after the electrode beveling. The EDX spectrum reveals the presence of Ni (0.85 and 7.45 keV), which was used as a metal catalyst in

the synthesis of the CNTs.^{34,38} The Al traces at 1.49 keV originate from the stage of the microscope.

Electrochemical Characterization. The electrochemical background scans (see Supporting Information, Figure S2) in phosphate buffered saline (PBS) and 0.1 M H₂SO₄ for a CNTF microelectrode and a conventional CF microelectrode showed that no significant peak corresponding to Ni was detected in the background scan in 0.1 M H₂SO₄. The lower limit of the potential window, -0.3 V in PBS and -0.1 V in 0.1 M H₂SO₄, was similar for both electrodes. The positive limit of the potential window differs significantly. The CNTF microelectrode has a lower positive potential limit of 0.7 V compared to the 1.0 V in the case of the CF microelectrode.

Typical CV traces obtained for different redox couples are presented in Figure 3A and B. The characteristic parameters obtained from these CVs are listed in Table 1. In the case of ruthenium hexaammine (RuHex) and ferrocenemethanol (FcMeOH), two outer-sphere redox couples, no significant difference could be observed between the two different materials. The double layer capacitance, obtained from the double layer part of the CV scans, did not change either, indicating that the surface areas of the electrodes are

Table 1. Results of the Electrochemical Characterization^a

redox probe	electrode	i_{dl}/nA	E_T/mV
RuHex (1 mM)	CNTF ($n = 5$)	-8.7 ± 1.3	53.4 ± 1.4
	CF ($n = 5$)	-10.4 ± 0.9	57.3 ± 6.1
FcMeOH (1 mM)	CNTF ($n = 5$)	7.0 ± 1.3	53.9 ± 2.8
	CF ($n = 5$)	8.5 ± 0.6	55.6 ± 1.9
DA (100 μM)	CNTF ($n = 5$)	1.5 ± 0.1	99.1 ± 10.9
	CF ($n = 4$)	1.4 ± 0.2	118.7 ± 21.6

^aCVs were performed in solutions of the different analytes listed on the table, dissolved in PBS (pH = 7.4). The scan rate was 10 mV s⁻¹. The data presented are the mean \pm standard deviation.

comparable (data not shown). Furthermore, the Tomes potential E_T

$$E_T = |E_{3/4} - E_{1/4}| \quad (1)$$

measured for these couples is consistent with a reversible reaction. For this type of couples, the Tomes criterion indicates that $E_T = 56.4/n$ where n is the number of electrons exchanged.³⁹ As shown in Figure 3C and D, the scan rate dependence for the reduction of RuHex at the CF and CNTF surfaces was investigated. At a scan rate higher than 50 mV s⁻¹, both electrodes show a macroelectrode behavior, and a peak of cathodic current can be defined. In particular, and for both materials, it was found that the peak current is linearly dependent on the square root of the scan rate, as expected for a diffusion controlled reaction, and the similar slopes for the two types of electrodes indicate similar diffusion profiles.

DA oxidation is known to be critically surface-dependent and thermodynamically irreversible, as demonstrated by the high E_T (Table 1). Calibration curves were plotted for DA (Figure 4A) and a linear fit ($R^2 = 0.9960$) was performed, as the diffusion limited current i_{dl} is linearly dependent on the analyte concentration.³⁹

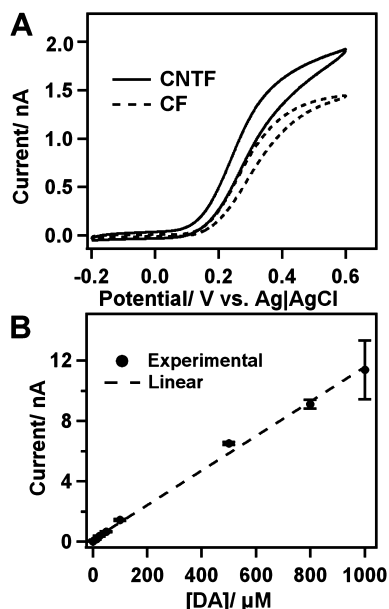


Figure 4. Electrochemistry of DA. A: typical CVs obtained in 100 μM DA in PBS buffer (pH 7.4) and B: calibration plot of the diffusion limited current (at 0.6 V vs Ag/AgCl) for DA.

Intrinsic RC Constant. Chronoamperometries between -0.2 and 0.4 V vs Ag/AgCl were run in PBS to investigate the discharge behavior of the materials. Indeed, both materials can show an intrinsic capacitance and resistance, in series, and can therefore behave as RC oscillators. This RC constant was calculated by fitting the discharge currents, shown in Figure 5, with a decaying exponentially:²⁷

$$f(t) = f_0 e^{-t/RC} \quad (2)$$

This RC constant was found to be significantly (1.29 ± 0.29 s vs 0.06 ± 0.08 s; $n = 4$, $p < 0.001$) higher for the CNT electrode. This was understood as evidence of the composite structure of this electrode, as incomplete contacts between two fibers can induce the formation of a capacitor. In addition, the

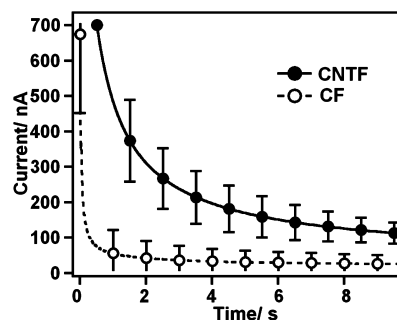


Figure 5. Chronoamperometric traces obtained in PBS, between -0.2 and 0.4 V vs Ag/AgCl. The data presented are the average ($\pm\text{S.D.}$, $n = 4$) discharge curves, obtained for CNTF (solid line) and CF (broken line) microelectrodes.

conductivity of CNT assemblies such as fibers is generally limited by the contact resistance of the nanotube junctions. As a result, CNT assemblies, in spite of the large conductivity of CNTs, are less conductive than bulk graphitic structures.

Resistance to Chemical Fouling. To assess the resistances of CNTF and CF electrodes against the chemical fouling of DA, steady state amperometric measurements with a working potential of 0.8 V vs Ag/AgCl were performed in PBS. The results are shown in Figure 6 for two concentrations, 1 mM (Figure 6A) and 100 μM (Figure 6B). The CNTF exhibited a significantly higher stability against chemical fouling caused by the oxidation products of the neurotransmitter in all tested cases. High DA concentrations, representing a worst-case scenario, blocked the electrode surface of CF very rapidly, as half of the initial steady state current is lost after $4\text{--}5$ min (t_{50} ,

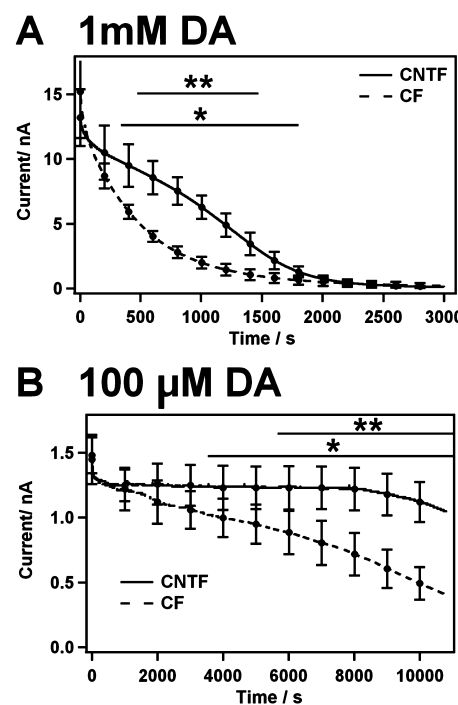


Figure 6. Effect of extended DA oxidation. Amperometric currents obtained for the oxidation at 0.8 V vs Ag/AgCl with the CNTF microelectrode (solid line) and CF microelectrode (broken line) of A: 1 mM DA and B: 100 μM DA in PBS buffer pH 7.4. Mean standard deviation, $n = 4\text{--}7$, the results were compared using Student's t test, *: $p < 0.05$; **: $p < 0.01$.

Table 2. Summary of the Fitting Values Based on the Model for the Amperometric Curves

	electrode	t_{50}/s	first slope/ A s^{-1}	second slope/ A s^{-1}	t_{zero}/s	$k/\text{m s}^{-1}$
1 mM DA	CNTF	917	-4.5×10^{-12}	-7.2×10^{-12}	1883	2.1×10^{-9}
	CF	283	-	-	-	-
100 μM DA	CNTF	13646	-6.0×10^{-15}	-7.6×10^{-14}	24742	1.6×10^{-10}
	CF	7945	-5.8×10^{-14}	-1.1×10^{-13}	14272	2.8×10^{-10}

indicating the time when the diffusion limited current i_{dl} has decreased by 50% (Table 2). The CNTF showed a better resistance with a t_{50} of 15 min.

The fouling of DA is assumed to be concentration dependent and lower concentrations indeed led to decreased chemical fouling. In the case of the lower DA concentration the CNTF retained the initial steady state current for two hours, whereas the CF showed a continuous signal decrease from the beginning, and during the same time under the same conditions the signal obtained at the CF decreased by almost 50%. After three hours of continuous oxidation of 100 μM DA the current decreased by only 15% in the case of CNTF and by 70% in the case of CF.

The DA fouling on the CNTF electrode surface occurred in two phases both using a high or a low concentration of DA. For high DA concentrations, the first phase is characterized by a slower blockage of the active electrode area. The second, faster, fouling phase leads to total blockage of the electrode surface. Also in the case of the CF two phases could be distinguished when using the low DA concentration. The two phasic fouling curves can be explained by the fact that the neurotransmitters need adsorption sites to be oxidized, thus leading to the formation of insulating patches, as detailed below.

Model of the Fouling Process and Kinetics. The data were fitted with the values obtained from the model presented in the Supporting Information, after normalization with the current obtained from the unblocked electrode. Different growth rates for $d(t)$ were tested, linear ($d = kt$), square ($d = kt^2$), and square root ($d = k\sqrt{t}$). As shown from Figure 7, the

second phase describes the fusion of the growing insulating layer leading to a complete blockage of the electrode surface.

Interestingly, the trace obtained for 1 mM DA with the CF electrode could not be fitted with this model. It is likely that the rapid decrease in current observed in this case prevents the formation of a stable depletion layer and rejects the steady-state hypothesis formed for this model (see the Supporting Information). The dynamic of the current decay is strongly controlled by the growth of the insulating layer. On the other hand, the CNTF electrode matched this model, indicating decreased growth of the insulating film and a substantial resistance to electrode passivation.

Table 2 summarizes the fitting values obtained with this model from the current traces showing a two-step decay. As the parameter t_{50} is 2 to 3 times larger for CNTF than for CF, for a fixed DA concentration and comparable current densities, this analysis strongly emphasizes the improved fouling resistance of CNTF over CF. The time t_{zero} was obtained by extrapolating the second tangent. This parameter gives an indication of the DA oxidation time required to record an almost null i_{db} i.e. that the electrode is fully blocked. At a 100 μM DA concentration, the t_{zero} of the CNTF is 74% higher than for the CF fiber. Additionally, for a DA level of 100 μM , the growth rate k obtained for the CNTF is 57% of the one measured for the CF, indicating that the insulating patches grow at a slower rate on the CNTF surface.

The current density of the CF and CNTF were comparable for the two concentrations of DA. Therefore, the rate of formation of o-DQ_x and the rate of polymerization of the insulating materials, should be comparable too, considering the reaction scheme of fouling (see Scheme 1). This fact indicates that the higher stability of CNTF arises from a decreased binding affinity of the insulating film to their surface. This phenomenon could also explain the improved resistance of the chemically stable synthetic diamond surfaces.⁴⁰ Furthermore, it has been suggested that CNTs offer a better resistance to electrode passivation thanks to their higher density of edge plane sites.³⁷ Altogether, these results indicate a higher resistance of the CNTF to fouling, thus longer and more reliable electrochemical measurements can be carried out, even in severe fouling conditions.

CONCLUSION

The CNTF microelectrodes presented here represent an attractive tool for steady state amperometry of neurotransmitters. They combine the high electroactivity and easy handling of CF electrodes with improved biochemical stability. Other CNT-based electrochemical devices have been proposed for electroanalysis, but the preparation requires heavy equipment and specialized facilities.^{13,22–28} The CNTF material presented here is a ready-to-use option, which does not require any additional modification or preactivation, in contrast with most of the recently reported CNT-based modifications.²⁶ Its fiber format will also facilitate its use in bioanalytical

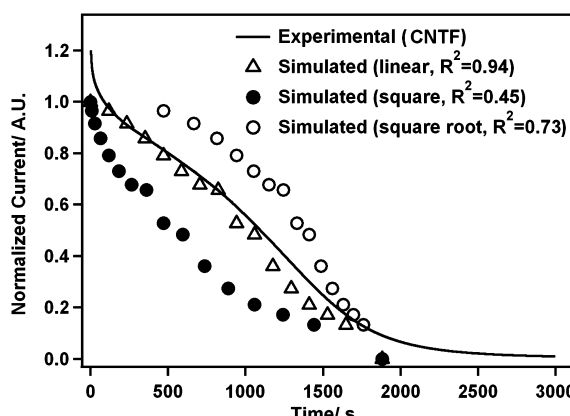


Figure 7. Model of the fouling process and kinetics. Fitting of the experimental data to the simulated current trace, for different types of growth of the insulating sites.

linear rate of growth of the insulating polymer gave the best fit to the experimental data ($R^2 = 0.94$), where $d = 2.1t$, in nm. This in particular indicates that the edge of the insulating patch progresses by 2.1 nm per second. According to this model, the first slower phase represents the growth of the insulating layer from the polymerization of the oxidation products. The faster

laboratories and could be a reliable alternative to the traditional CF.

ASSOCIATED CONTENT

Supporting Information

Additional information as noted in text. This material is available free of charge via the Internet at <http://pubs.acs.org>.

AUTHOR INFORMATION

Corresponding Author

*Phone +46 766 22 90 61. E-mail: gulnara.safina@chem.gu.se.

Present Address

[§]Lohmann & Rauscher GmbH, 2525 Schönau an der Triesting, Austria.

Notes

The authors declare no competing financial interest.

ACKNOWLEDGMENTS

The authors wish to thank Jani Tuoriniemi for technical assistance during the SEM/EDX measurements. The work has been supported by the European Research Council (Advanced Grant), the Knut and Alice Wallenberg Foundation, the Swedish Research Council (VR), The Royal Society of Arts and Sciences in Gothenburg and the National Institutes of Health. G.S. has been supported by a Young Investigator Project Grant from VR and by a grant from the Ångpanneföreningen's Foundation for Research and Development.

REFERENCES

- (1) Sulzer, D. *Neuron* **2011**, *69*, 628–649.
- (2) Berridge, K. C.; Robinson, T. E. *Brain Res. Rev.* **1998**, *28*, 309–369.
- (3) Adams, R. *Anal. Chem.* **1976**, *48*, 1126A–1138A.
- (4) Robinson, D. L.; Hermans, A.; Seipel, A. T.; Wightman, R. M. *Chem. Rev.* **2008**, *108*, 2554–2584.
- (5) Staal, R. G. W.; Rayport, S.; Sulzer, D. In *Electrochemical Methods for Neuroscience*; Michael, A. C., Borland, L. M., Eds.; CRC Press: Boca Raton, FL, 2007.
- (6) Robinson, D. L.; Venton, B. J.; Heien, M. L. A. V.; Wightman, R. M. *Clin. Chem.* **2003**, *49*, 1763–1773.
- (7) Keithley, R. B.; Takmakov, P.; Bucher, E. S.; Belle, A. M.; Owesson-White, C. A.; Park, J.; Wightman, R. M. *Anal. Chem.* **2011**, *83*, 3563–3571.
- (8) Cahill, P. S.; Walker, Q. D.; Finnegan, J. M.; Mickelson, G. E.; Travis, E. R.; Wightman, R. M. *Anal. Chem.* **1996**, *68*, 3180–3186.
- (9) Hawley, M. D.; Tatawadhi, S. V.; Piekarzki, S.; Adams, R. N. J. *Am. Chem. Soc.* **1967**, *89*, 447–450.
- (10) Tse, D. C. S.; McCreery, R. L.; Adams, R. N. *J. Med. Chem.* **1976**, *19*, 37–40.
- (11) Wrona, M. Z.; Lemordant, D.; Lin, L.; Blank, C. L. R.; Dryhurst, G. *J. Med. Chem.* **1986**, *29*, 499–505.
- (12) Wrona, M. Z.; Dryhurst, G. *Bioorg. Chem.* **1990**, *18*, 291–317.
- (13) McCreery, R. L. *Chem. Rev.* **2008**, *108*, 2646–2687.
- (14) Gonon, F.; Buda, M.; Cesuglio, R.; Jouvet, M.; Pujol, J. F. *Nature* **1980**, *286*, 902–904.
- (15) Huffman, M. L.; Venton, B. J. *Analyst* **2009**, *134*, 18–24.
- (16) DuVall, S.; McCreery, R. J. *Am. Chem. Soc.* **2000**, *122*, 6759–6764.
- (17) Heien, M. L. A. V.; Phillips, P. E. M.; Stuber, G. D.; Seipel, A. T.; Wightman, R. M. *Analyst* **2003**, *128*, 1413–1419.
- (18) Hashemi, P.; Dankoski, E.; Petrovic, J.; Keithley, R.; Wightman, R. *Anal. Chem.* **2009**, *81*, 9462–9471.
- (19) Singh, Y. S.; Sawarynski, L. E.; Dabiri, P. D.; Choi, W. R.; Andrews, A. M. *Anal. Chem.* **2011**, *83*, 6658–6666.
- (20) Sarada, B. V.; Rao, T. N.; Tryk, D. A.; Fujishima, A. *J. Electrochem. Soc.* **1999**, *146*, 1469–1471.
- (21) Xu, J.; Chen, Q.; Swain, G. M. *Anal. Chem.* **1998**, *70*, 3146–3154.
- (22) Musameh, M.; Wang, J.; Merkoci, A.; Lin, Y. *Electrochim. Commun.* **2002**, *4*, 743–746.
- (23) Dumitrescu, I.; Unwin, P. R.; Macpherson, J. V. *Chem. Commun.* **2009**, *6886*–6901.
- (24) Nayagam, D. A. X.; Williams, R. A.; Chen, J.; Magee, K. A.; Irwin, J.; Tan, J.; Innis, P.; Leung, R. T.; Finch, S.; Williams, C. E.; Clark, G. M.; Wallace, G. G. *Small* **2011**, *7*, 1035–1042.
- (25) Pumera, M. *Chem.—Eur. J.* **2009**, *15*, 4970–4978.
- (26) Swamy, B. E. K.; Venton, B. J. *Analyst* **2007**, *132*, 876–884.
- (27) Dumitrescu, I.; Edgeworth, J. P.; Unwin, P. R.; Macpherson, J. V. *Adv. Mater.* **2009**, *21*, 3105–3109.
- (28) Güell, A. G.; Meadows, K. E.; Unwin, P. R.; Macpherson, J. V. *Phys. Chem. Chem. Phys.* **2010**, *12*, 10108–10114.
- (29) Lu, W.; Zu, M.; Byun, J. H.; Kim, B. S.; Chou, T. W. *Adv. Mater.* **2012**, *24*, 1805–1833.
- (30) Hu, L.; Hecht, D. S.; Grüner, G. *Chem. Rev.* **2010**, *110*, 5790–5844.
- (31) Zhou, X.; Boey, F.; Zhang, H. *Chem. Soc. Rev.* **2011**, *40*, 5221–5231.
- (32) Viry, L.; Derré, A.; Poulin, P.; Kuhn, A. *Phys. Chem. Chem. Phys.* **2010**, *12*, 9993–9995.
- (33) Wang, J.; Deo, R.; Poulin, P.; Mangey, M. *J. Am. Chem. Soc.* **2003**, *125*, 14706–14707.
- (34) Vigolo, B.; Pénicaud, A.; Coulon, C.; Sauder, C.; Pailler, R.; Journet, C.; Bernier, P.; Poulin, P. *Science* **2000**, *290*, 1331–1334.
- (35) Hochstetler, S.; Wightman, R. In *On-Line Biophysics Textbook*; Bloomfield, V., De Felice, L., Eds.; Biophysical Society: Bethesda, MD, 1998.
- (36) Kawagoe, K. T.; Zimmerman, J. B.; Wightman, R. M. *J. Neurosci. Methods* **1993**, *48*, 225.
- (37) Banks, C. E.; Compton, R. G. *Analyst* **2005**, *130*, 1232–1239.
- (38) Poulin, P.; Vigolo, B.; Launois, P. *Carbon* **2002**, *40*, 1741–1749.
- (39) Bard, A. J.; Faulkner, L. R. *Electrochemical methods: fundamentals and applications*, 2nd ed.; Wiley: New York, 1980.
- (40) Trouillon, R.; O'Hare, D. *Electrochim. Acta* **2010**, *55*, 6586–6595.